25th ABCM International Congress of Mechanical Engineering
October 20-25, 2019, Uberlândia, MG, Brazil

COB-2019-2226
NUMERICAL SHAPE OPTIMIZATION OF AIRFOIL USING IMERSPEC AND RESPONSE SURFACE METHODOLOGIES TO FLOW AT LOW REYNOLDS NUMBER

Lucas Marques Monteiro
Andreia Aoyagui Nascimento
Felipe Pamplona Mariano
Universidade Federal de Goiás (UFG) – Escola de Engenharia Elétrica, Mecânica e de Computação (EMC) – Laboratório de Engenharia Térmica e de Fluidos (LATEF), Av. Universitária, 1488, Bloco A, Piso: 3, Setor Leste Universitário, CEP: 74605-010, Goiânia – GO – https://latef.emc.ufg.br/
lucasescorpi@gmail.com; aanascimento@ufg.br; fpmariano@ufg.br

Abstract. *The objective of the present work is evaluating the influence of the shape of the airfoils, determining their aerodynamic parameters as lift and drag coefficients and aerodynamic efficiency. For this purpose, the fluid flow over NACA 0008 and NACA 2408 were simulated for Re_c equal to 2000, using the IMERSPEC methodology, resulting from the coupling of the Fourier Pseudo-Spectral Method and the Immersed Boundary Method. In order to guarantee convergence between the results of the present work and the data available in the literature the mesh refinement and changes in number of numerical interactions are made, by resulting an improvement of the accuracy. The occurrence of phenomena such as the intensification of the adverse pressure gradient and the vortex shedding were observed. Finally, using the Response Surface Methodology (RSM), the NACA 2408 airfoil shape optimization was proposed. These procedures resulted an increase in aerodynamic efficiency. Based on these analyzes, one can show the advantage of the IMERSPEC methodology to understand the behavior of flow over aerodynamic bodies. Associating it with the RSM methodology allowed to estimate, with reliability, the optimal design of new airfoil profile, without the need to perform many numerical simulations.*

Keywords: *Computational Fluid Dynamic, Flow over Airfoils, Optimization, Response Surface Methodology, IMERSPEC Methodology*

1. INTRODUCTION

High order methods provide an excellent accuracy to study several problems in Computational Fluids Dynamics (CFD) (Uhlmann, 2005 and Wang et al. 2008). High order finite differences methods and compact schemes (Briggs and Henson, 1995) are methods that obtain excellent results to study phenomena involving aeroacustic, transition to turbulence and combustion. On the other hand, they have disadvantaged of computational expensive cost in comparison to conventional methods (Mariano *et al.*, 2010).

The advents of spectral methods become possible to joining high accuracy with low computational cost (Canuto *et al.*, 2006) in comparison with another high order methods. This relative low cost is given by the Fast Fourier Transform (FFT) (Briggs and Henson, 1995), since the cost of a problem resolution with finite differences is order of $O(N^2)$, where N is the number of the grid points, the cost of the FFT is of $O(Nlog2N)$. Furthermore, it was also developed the projection method (Canuto *et al.* 2006), which gives the pressure field in the spectral space. Using the projection process is not necessary to calculate the Poisson equation, as it is done by conventional methodologies to solve incompressible fluid flows. The disadvantage of the spectral methodology is the difficulty to work with complex geometries and boundary conditions.

One of the most practical methodologies to work with complex and moving geometries is the Immersed Boundary (IBM) (Peskin, 2002). It is characterized by the imposition of a term source, which has the role of a body force added to the Navier-Stokes equations, to model virtually a body immersed in the flow. The aims of this term are to represent the boundary conditions of the immersed geometry as a body force (Griffith and Peskin, 2005).

The methodology, presented in the present paper, works with Fourier Pseudo-Spectral Method connected with Immersed Boundary Method to simulate flows over airfoil and to optimize the shape of an airfoil at low Reynolds number to increase the aerodynamic efficiency. The optimized problem is solved by using the Response Surface Methodology (RSM), that using few complete CFD simulations and obtain the algebraic equation (metamodel) to perform the optimization process.

2. METHODOLOGY

This section presents the mathematic model to dynamic of incompressible fluid flow and the immersed boundary method to impose the boundary conditions in physical space. Next subsection, it presents the transformed from this physical model to Fourier spectral space. The last subsection presents the Response Surface Methodology (RSM) applied in optimization airfoil shape.

2.1 Mathematic model for the fluid

The flow is represented by momentum equations (Eq. 1) and the continuity equation (Eq. 2). The information of the fluid/solid interface (domain Γ in Fig. 1) is transposed to the Eulerian domain (Ω in Fig. 1) for addition of the term source, f_l, in the Navier-Stokes equations. The objective of this term is to represent the boundary conditions of the immersed geometry as a body force (Goldstein *et al.*,1993). The Navier-Stokes equations are presented in theirs tensorial form:

$$\frac{\partial u_l}{\partial t} + \frac{\partial (u_l u_j)}{\partial x_j} = -\frac{\partial p}{\partial x_l} + \nu \frac{\partial^2 u_l}{\partial x_j \partial x_j} + f_l, \tag{1}$$

$$\frac{\partial u_j}{\partial x_j} = 0, \tag{2}$$

where $\frac{\partial p}{\partial x_l} = \frac{1}{\rho_f}\frac{\partial p^*}{\partial x_l}$; p^* is the static pressure in [N/m^2]; u_l is the velocity in l direction in [m/s]; $f_l = \frac{f_l^*}{\rho_f}$; f_l^* is the term source in [N/m^3]; ρ_f is the density; ν is the kinematic viscosity in [m^2/s]; x_l is the spatial component (x,y) in [m] and t is the time in [s]. The initial condition is any velocity field that satisfies the continuity equation, Eq. (2).

The source term is defined in eulerian domain, Ω, but it has different values from zeros only in the points which coincide with the immersed geometry, it enables that the Eulerian field perceives the presence of solid interface (Enriquez-Remigio and Silveira Neto, 2007).

$$f_l(\vec{x},t) = \begin{cases} F_l(\vec{x}_k,t) & \text{if } \vec{x} = \vec{x}_k \\ 0 & \text{if } \vec{x} \neq \vec{x}_k \end{cases}, \tag{3}$$

where $\vec{x}$ is the position of the particle in the fluid and $\vec{x}_k$ is the position of a point in solid interface (Fig. 1).

The boundary conditions are periodic in all directions in Eulerian domain, Ω_B, as showed in Fig. 1, it is necessary due to Fourier pseudo-spectral method properties. The boundary condition is imposed by direct forcing method in Γ_{BC}, and the boundary conditions of bodies immersed in flow, represented by Γ_i in Fig. 1.

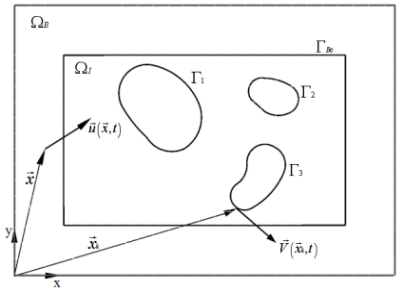

Figure 1. Schematically representation of eulerian and lagrangian domain.

Using Eq. (3) can be concluded that the field $f_l(\vec{x},t)$ is discontinuous, which can be numerically solved only when there is coincidence between the points that compose the interface domain with the points that compose the fluid domain. In the cases there is no coincidence between these points, very frequently in the complex geometries, it is necessary to distribute the function $f_l(\vec{x},t)$ over its neighborhoods. Just by calculating the lagrangian force field $F_l(\vec{x}_k,t)$, it can be distributed and thus, transmitted the information geometry presence for Eulerian domain, these functions can be found in Griffith and Peskin, (2005).

2.2. Mathematic model for the immersed interface

The lagrangian force field is calculated by direct forcing method, which was proposed by Uhlmann (2005). One of the characteristics of this model is that is not necessary using *ad-hoc* constants and allows the modeling non-slip condition on immersed interface. The lagrangian force $F_l(\vec{x}_k,t)$ is available by momentum conservation equation over a fluid particle that is joined in the fluid-solid interface:

$$F_l(\vec{x}_k,t)=\frac{\partial u_l}{\partial t}(\vec{x}_k,t)+\frac{\partial}{\partial x_j}(u_l u_j)(\vec{x}_k,t)+\frac{\partial p}{\partial x_l}(\vec{x}_k,t)-\nu\frac{\partial^2 u_l}{\partial x_j \partial x_j}(\vec{x}_k,t). \tag{4}$$

The values of $u_l(\vec{x}_k,t)$ and $p(\vec{x}_k,t)$ are done by interpolation of velocities and pressure, respectively, of Eulerian points near the immersed interface. For lagrangian points, x_k, at the immersed boundary, we have:

$$F_l(\vec{X}_k,t)=\frac{u_l(\vec{x}_k,t+\Delta t)-u_l^*(\vec{x}_k,t)+u_l^*(\vec{x}_k,t)-u_l(\vec{x}_k,t)}{\Delta t}+RHS_l(\vec{x}_k,t), \tag{5}$$

where u^* is a temporary parameter (Wang, *et al.* 2008), Δt is the time step and $RHS_l(\vec{x}_k,t)=\frac{\partial}{\partial x_j}(u_l u_j)(\vec{x}_k,t)+\frac{\partial p}{\partial x_l}(\vec{x}_k,t)-\nu\frac{\partial^2 u_l}{\partial x_j \partial x_j}(\vec{x}_k,t)$.

The Eq. (5) is solved by Eqs. (6) and (7) at same time step:

$$\frac{u_l^*(\vec{x}_k,t)-u_l(\vec{x}_k,t)}{\Delta t}+RHS_l(\vec{x}_k,t)=0, \tag{6}$$

$$F_l(\vec{x}_k,t)=\frac{u(\vec{x}_k,t+\Delta t)-u_l^*(\vec{x}_k,t)}{\Delta t}, \tag{7}$$

where $u(\vec{x}_k,t+\Delta t)=U_{FI}$ is the immersed boundary velocity.

Eq. (6) is solved at eulerian domain at Fourier spectral space, *i.e.* the solution of Eq. (1) with $f_l=0$. $u_l^*(\vec{x},t)$ is interpolated for lagrangian domain, became $u_l^*(\vec{x}_k,t)$ and it is computed on Eq. (7). Then, the lagrangian force, $F_l(\vec{x}_k,t)$, is smeared for eulerian mesh. Finally, the velocity is update by Eq. (8):

$$u_l(\vec{x},t+\Delta t)=u_l^*(\vec{x},t)+\Delta t.f_l. \tag{8}$$

2.3. Fourier Pseudo-Spectral Method

By defining the equations that govern the flow through IBM, the next step is transforming them to the Fourier spectral space. The Fourier transformed is applied in the continuity equation, Eq. (2), we obtain:

$$ik_j\hat{u}_j=0. \tag{9}$$

The scalar product between two vectors is null, if both are just orthogonal. Therefore, from Eq. (9), the wave number vector k_j is orthogonal to transformed velocity $\hat{u}_j$. The plane of divergent free (plane π) is defining, perpendicular to wave number vector $\vec{k}$ and thus, transformed velocity vector $\hat{\vec{u}}(\vec{k},t)$ belongs to plane π.

Now applying the Fourier transform in the momentum equation Eq. (2), we obtain:

$$\frac{\partial \hat{u}_l^*}{\partial t}+ik_j u_l^* u_j^*=-ik_l\hat{p}-\nu k^2\hat{u}_l^*+\hat{f}_l, \tag{10}$$

where k^2 is the square norm of wave number vector, *i.e.*, $k^2=k_jk_j$. and $i=\sqrt{-1}$.

In agreement of the plane π definition, each one of the terms of Eq. (10) assumes a position related to it: the transient term and the viscous term belong to the plane π. The gradient pressure term is perpendicular to plane π and the non-linear and force terms, a priori, they are not known in which position it can be found in relation to plane π. By joining the terms of Eq. (10) and observing the definition of plane π, we have found that,

$$\underbrace{\left[\frac{\partial \hat{u}_l^*}{\partial t} + \nu k^2 \hat{u}_l^*\right]}_{\in\pi} + \underbrace{\left[ik_j u_l^* u_j^* + \hat{f}_l + ik_l \hat{p}\right]}_{\in\pi} = 0. \quad (11)$$

To solve Eq. (11) is needed that the non-linear and the force field terms are over plane π. For that, it is utilized projection tensor definition (Canuto *et al*., 2007), which projects any vector over it. Therefore, applying this definition on the right-hand side of the sum done in Eq. (11):

$$\left[ik_j u_j^* u_l^* + ik_l \hat{p}\right] = \wp_{lm}\left[ik_j u_m^* u_l^* + \hat{f}_l\right]. \quad (12)$$

The term of the gradient pressure is orthogonal to plane π, then, it is zero after to be projected, disentailing from calculates of Navier-Stokes equations in the spectral space. The pressure field can be recovered at the post-processing manipulating Eq. (12) (Canuto *et al*., 2006).

Other important point is the non-linear term, in which appears the product of transformed functions, in agreement with Fourier transformed properties, this operation is a convolution product and its solution is given by convolution integral, this is solved by Pseudo-Spectral Fourier Method (Canuto *et al*., 2007). Therefore, the momentum equation in the Fourier space, using the method of the projection, assumes the following form:

$$\frac{\partial \hat{u}_l^*\left(\vec{k},t\right)}{\partial t} + \nu k^2 \hat{u}_l^*\left(\vec{k},t\right) = -ik_j \wp_{lm}\left[\hat{f}_l + \int_{\vec{k}=\vec{r}+\vec{s}} \hat{u}_m^*\left(\vec{r},t\right)\hat{u}_l^*\left(\vec{k}-\vec{r},t\right)d\vec{r}\right]. \quad (13)$$

Non-linear term can be handed by different forms: advective, divergent, skew-symmetric, or rotational (Canuto *et al*., 2006), in spite of being the same mathematically, they present different properties when discretized. The skew-symmetric form is more stable and present best results but is twice more onerous that the rotational form. However, this inconvenience can be solved using the alternate skew-symmetric form, it is consisting in alternate between the advective and divergent forms in each time step (Souza, 2005), it is proceeding adopted for this paper.

For all types of handing the non-linear term is necessary solve the convolution integral, but its numerical solution is computational expensive, then the Pseudo-Spectral Method is used, *i.e.* to calculate the velocity product in the physical space and to transform this product for the spectral space.

When solved numerically the Navier-Stokes equations with the Fourier spectral method using the Discrete Fourier Transform (DFT), which is define by Briggs and Henson (1995):

$$f_k = \sum_{n=-N/2+1}^{N/2} f_n e^{\frac{-i2\pi kn}{N}}, \quad (14)$$

where k is wave number, N is number of meshes points, n get the position x_n of collocation points ($x_n=n\Delta x$).

The DFT restriction is periodic boundary conditions, by limiting the use of Fourier spectral transformed for CFD problems. The advantage is low computational cost gives by Fast Fourier Transform (FFT) (Cooley and Tukey, 1965), which solves the DFT (Eq. 19) of a way very efficiently, order *O(Nlog2N)*. For systems with many collocation points, *e.g.* three-dimensional problems, the spectral method is very cheap when compared with another conventional high order methodologies.

2.4. Proposed Methodology: IMERSPEC

The algorithm of IMERSPEC method purposed is:

1) Solve the Eq. (13) in Fourier spectral space, without force term, and obtain the temporal parameter $\hat{u}^*\left(\vec{k},t\right)$, using the low dispersion and low storage Runge-Kutta method proposed by Allampalli *et al*., (2009);

2) Use the Inverse Fast Fourier Transformer in $\hat{u}^*\left(\vec{k},t\right)$ and obtain $u^*\left(\vec{x},t\right)$ at physic space in the domain Ω;

3) Interpolate $u^*(\vec{x},t)$ for the lagrangian domain by cubic function proposed by Griffith and Peskin (2005), and obtain $u^*(\vec{x}_k,t)$;

4) Calculate the lagrangian force, $F_l(\vec{x}_k,t)$, by Eq. (7);

5) Update particles velocity;

6) Distribute the $F_l(\vec{x}_k,t)$ by cubic function proposed by Griffith and Peskin (2005), and obtain $f(\vec{x}_k,t)$ in eulerian domain;

7) Update the eulerian velocity, $u(\vec{x},t)$ by Eq. (8) and transformed it using FFT for spectral space, $\hat{u}^*(\vec{k},t)$, returned by step 1.

2.5. Flow over an immersed body

An inlet profile flow is imposed with uniform velocity U_∞ in [*m/s*] and the flow cross the section of an airfoil (Fig. 2). The flow produces two hydrodynamic forces, lift and drag. The respectively coefficients of these forces are *Cd* and *Cl*, given by Eqs. (15) and (16). These variables determine the forces that act on bodies immersed in flow, the drag coefficient determines the resistance force of the fluid on the body immersed, while the lift coefficient determines the force that have in the direction perpendicular to incoming flow, the one of the main problems of aeronautical engineering is the optimization of shape of the airfoils, that consist in maximize the lift and minimized the drag of the airfoil profiles.

$$Cd = \frac{-2\sum F_x}{\rho U_\infty^2 c}, \tag{15}$$

$$Cl = \frac{-2\sum F_y}{\rho U_\infty^2 c}, \tag{16}$$

where: F_x and F_y are the forces calculated at each lagrangean point with the sum of the forces each lagrangean point obtained by Eq. (7); *c* is the cord of airfoil.

The calculus domain, we used the 1024x256 collocation points in eulerian domain and 1000 points to discretize the lagrangen domain, *i.e.*, the airfoil. The simulations reach 75 s of physical time and reach the stead state.

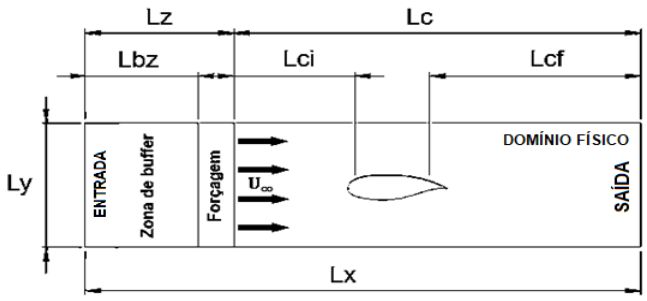

Figure 2. Schematically representation of eulerian and lagrangian domain.

Periodicity conditions were used at the top and bottom boundary of the domain. The inflow condition is a uniform profile of velocity (U_∞=*1,0 m/s*), imposed by immersed boundary. A buffer zone was also used as Uzun, (2003):

$$ZB = \phi(Q_l - Qt_l) \tag{17}$$

where *Q* is the problem solution, that is, *u* and v, *Qt* is the target solution, which is required in the final buffer zone. In the present case, the target solution is a uniform profile U_∞, and ϕ is a parameter of vortex stretching, and it is calculated by Eq. (18):

$$\phi_\eta = \beta\left(\frac{x_\eta - x_{ZB}}{x_f - x_{ZB}}\right)^\alpha, \tag{18}$$

where $\alpha=3.0$ and $\beta=1.0$ (Uzun, 2003), x_{ZB} and x_f give the length of the buffer zone, respectively, x_η is a generic position.

The inflow condition is a uniform profile of velocity ($U_\infty=1,0$ *m/s*). Other important parameter is the Reynolds number, that is *Re=2000*. With the number of Reynolds is possible to determine the viscosity of the fluid:

$$\nu = \frac{U_\infty D}{\mathrm{Re}} \tag{19}$$

2.6. Response Surface Methodology

Response surface methodology (RSM) (Barros Neto, *et al.*, 2001) is an optimization method based on factorial design. This is an optimization process based on metamodel, where it proposes to replace complex high order models with low order models (metamodels). Thus, the computational effort can be reduced and the reality of the physical problem can be reliably and accurately represented.

The mathematical formulation of the RSM optimization is dealt with in this section, addressing the assembly of the factor planning matrix, the generation of the airfoils that make up the matrix, the proposition of the mathematical model adjustment and the evaluation of the models by the analysis of variance technique (ANOVA).

2.6.1. Generation of the airfoils

For the generation of the airfoils that make up the planning matrix, the camber line of the NACA 2408 base airfoil was discretized into 6 points, 4 points are fixed (anchored) and their coordinate values will not change from the camber line of the original NACA 2408 airfoil.

The other 2 points, variables, are the free points that will vary in their value according to the levels defined by the study of this work. Figure 3 shows the discretized coordinates, where the squares nodes from 1 to 4 are the fixed points and the circular nodes are the variable points.

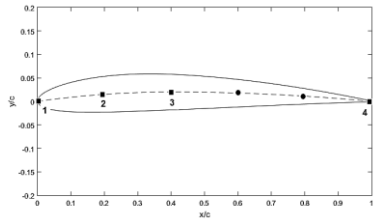

Figure 3. NACA 2408 camber line discretized.

The free points are the factors (manipulated variables) of the planning matrix, they are located at x/c = 0.6 and x/c = 0.8 of the camber line and will be called factor A and factor B. Their coordinates in y/c will vary by the levels of the problem. To identify the levels, the sample space of the problem is defined, given by Eq. 20. and Eq. 21:

$$0 \leq A \leq 0{,}02 \rightarrow -1 \leq A \leq 1 \tag{20}$$

$$0 \leq B \leq 0{,}02 \rightarrow -1 \leq B \leq 1 \tag{21}$$

With sample space it is possible to show that the y/c coordinates of the camber free points will range from 0 to 0.02, which is the maximum curvature thickness of the original NACA 2408 airfoil. The left side of Eq. 20 and Eq. 21 represents the real limits of the sample space and the right side the limits in their normalized form.

The levels were defined according to the normalization of Eq. 21 and Eq. 22 and considering a central point between the limits of the sample space. Therefore, the levels at which the factors will be subject to variation are -1, 0 and 1, where: 1 represents y/c = 0, 0 represents y/c = 0.01 and 1 is y/c = 0.02 of camber line.

The proposed problem has 2 factors and 3 distinct levels. Therefore, we have the complete factorial design matrix 3^2, totaling 9 distinct combinations. Table 1 shows the complete normalized factorial design matrix and its combinations. The planning matrix shows the y/c coordinate values of the free points (factors A and B of the Eqs. 20 and 21) in each combination. For example, for combination 01, the fixed points of the camber line will have their coordinates defined as shown in Fig. 3 and are invariable. Free points, x/c = 0.6 will have y/c = 0 and at x/c = 0.8, y/c = 0. For combination 02, free points, x/c = 0.6 will have y/c = 0.01 and at x/c = 0.8, y/c = 0.01. For combination 03, the free points, x/c = 0.6 will have y/c = 0.02 and at x/c = 0.8, y/c = 0.02 and so on.

The six discretized points of the camber line form a data set that varies as a function of free points. Each data set, defined by matrix combinations, represents the drawing of a camber line of a new airfoil.

The curves of the camber line of the airfoils were adjusted using the least-squares error-minimizing polynomial regression technique. For each camber line, the coefficients of a 5th order polynomial *y/c = f (x/c)* that best fit the points defined in each data set were determined.

Table 1. Full factorial design matrix normalized.

Combination	Factor A	Factor B
01	-1	-1
02	0	0
03	1	1
04	-1	0
05	-1	1
06	1	0
07	1	-1
08	0	1
09	0	-1

The upper surface, lower surface and thickness of the new airfoils were obtained using the mathematical modeling proposed to obtain the four-digit NACA airfoil (Monteiro, 2018; Dheepak *et al*., 2015) and depend on the discretization of the polynomial functions *y/c = f (x / c)* representing the camber line. The curve was discretized at 500 points. The airfoils obtained for each combination of the planning matrix were illustrated in Fig. 4.

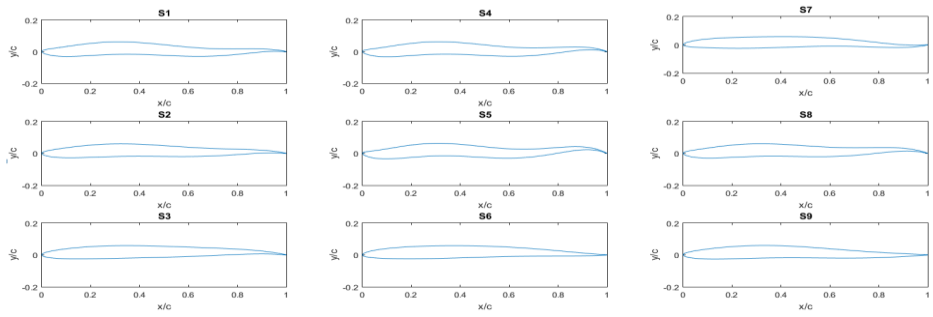

Figure 4. Aerodynamic profiles generated by the planning matrix.

2.6.2. Metamodeling and analysis of variance (ANOVA)

The models (metamodels) are represented by regression curves given by polynomial functions in their matrix form:

$$\mathbf{Y} = \mathbf{X}\beta + \phi, \tag{22}$$

where *Y* is the model response, *X* is the model factors and their interactions, β are the model coefficients and ϕ are the random errors associated with numerical simulations.

A quadratic metamodel was adjusted with interaction between factors A and B, given by Eq. 23:

$$\mathbf{X} = [1 \quad \mathbf{A} \quad \mathbf{B} \quad \mathbf{AB} \quad \mathbf{AB^2}], \tag{23}$$

where A is the vector given by factor A levels, B is the vector given by factor B levels in the factorial design matrix, as shown in Tab. 2. AB is the point-to-point multiplication between factor A vector and the factor B and AB² vector is the point-to-point multiplication between the factor A vector and the factor B squared vector.

The coefficients β are given by the least squares method according to Eq. 24:

$$\beta=(\mathbf{X}^T\mathbf{X})^{-1}\mathbf{X}^T\mathbf{Y}, \tag{24}$$

where, $\mathbf{X}^T$ is the transpose matrix of **X**, the exponent *-1* represents the inverse matrix of the product ($\mathbf{X}^T\mathbf{X}$) and Y are the answers obtained by numerical simulations (aerodynamic coefficients).

Random errors of numerical simulations will be quantified by the ANOVA technique and can be nullified from Eq. 22. Therefore, replacing Eq. 24 in Eq. 22, the simplified curve that adjusts the metamodel is given by Eq. 25.

$$Y=[(\mathbf{X}^T\mathbf{X})^{-1}\mathbf{X}^T\mathbf{Y}]X \tag{25}$$

Given the adjusted metamodel, its quality and its ability to represent the proposed physical model should be evaluated, quantifying its errors and residuals using the variance analysis technique (ANOVA). The objective is to analyze the sensitivity level of the variables and their sensitivity of the model factors. Table 02 shows the simplified ANOVA table (Monteiro, 2018) that was used for metamodel validation in the present work.

Table 2. Table of simplified ANOVA.

Factor	Sum of squares	Degrees of freedom	Mean square
Regression	$SQ_R = \sum_i^m \sum_j^{n_i} \left(y_i - \bar{y}\right)^2$	p-1	$MQ_R = \frac{SQ_R}{p-1}$
Error	$SQ_r = \sum_i^m \sum_j^{n_i} \left(\hat{y} - y_i\right)^2$	n-p	$MQ_r = \frac{SQ_r}{n-p}$

where n is the total number of observations made by the tests, p is the number of model parameters (number of matrix elements of Eq. 24) and m is the number of distinct levels of the independent variables. SQ_T refers to variations in experimental observations $\hat{y}$, due to the adjusted regression (SQ_R) equation and due to residuals (SQ_r) around the overall mean (mean of test results) $\bar{y}$. The results regarding the model is y_i.

From the ANOVA, the F test (Galdámez, 2002) is used to validate the adjusted metamodels ensuring their statistical evidence and representativeness if $MQ_R / MQ_r > F_{p-1,\, n-p}$.

F is the Fisher-Snedecor distribution function given at a percentage reliability level and as a function of the degrees of freedom of the source of variation with respect to regression and residuals. A well-adjusted model is one in which the share of change due to regression is greater than the share of change due to residuals.

3. RESULTS

This section presents the simulations of flows over airfoils NACA0008 with two refinement mesh, such that the validation of numerical code is done. And, the second part, we present the process of shape optimization of the airfoil NACA2408 using RMS technique.

3.1. Mesh Refinement

The mesh refinement simulations are set until $t = 300$ s. The inlet profile velocity is $U_\infty = 1{,}0$ m/s and the Reynold number is $Re_c = 2000$. The lagrangian mesh of the airfoil is defined as $\Delta s = \Delta x$, *i.e.*, to the mesh of the 512x128 eulerian points has 97 lagrangian points and to the mesh of the 1024x256 eulerian points has 193 lagrangian points equally spaced over the airfoil surface.

Figure 5 show the vorticity field over the airfoil NACA 0008, in angle of attack of 4º, with the two different meshes. Figure 5(a) show the vortex shedding caused to the coarse mesh numerical errors, and the Fig. 5(b) does not exist the vortex shedding, presenting the importance of refinement of grid.

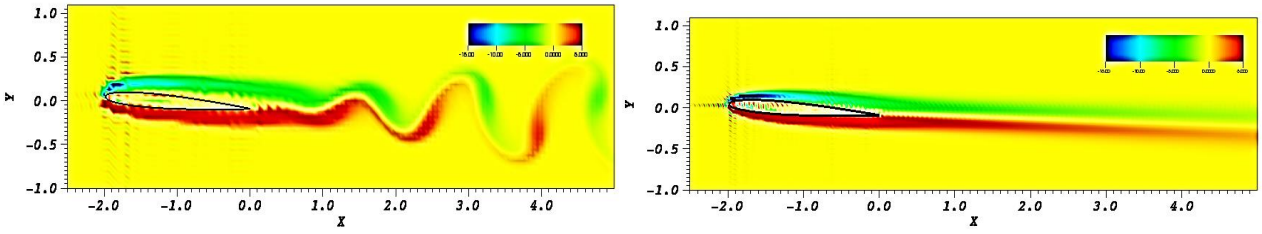

(a) (b)

Figure 5. Vorticity field over the airfoil NACA0008 in the t=300 s to meshes (a) 512x128 and (b) 1024x256.

Table 3 shows the temporal mean of lift and drag coefficients in comparison with the Kunz and Kroo (2001) and Mittal *et al*. (2008).

3.2 Shape airfoil optimization process

We perform nine flow simulations, using IMERSPEC methodology (Mariano *et al*., 2010), over each airfoil of the Fig. 4, using 1024 x 256 collocation points and we calculate the mean temporal of drag and lift coefficients between 75 s until 300 s. All airfoils are at the angle of attack of 0º. The Tab. 4 present the mean temporal of drag and lift coefficients obtained in each simulation.

Table 3. Temporal mean of lift and drag coefficients of airfoil NACA0008 in the angle of attack of 4º.

Mesh	C_L	C_D	C_L/C_D
512x128	0,2028	0,1058	1,9168
1024x256	0,2494	0,0878	2,8405
Mittal *et al.* (2008)	0,2730	0,0810	3,3703
Kunz and Kroo (2001)	0,2720	0,0800	3,3400

Table 4 - Mean temporal of lift (C_L) and drag (C_D) coefficients obtained in each flow simulation of the Fig. 4.

Simulation	C_L	C_D
01	0,0340	0,0910
02	0,0556	0,0905
03	0,0785	0,0900
04	0,0116	0,0873
05	-0,0153	0,0901
06	0,0641	0,0858
07	0,0783	0,0871
08	0,0245	0,0873
09	0,0512	0,0854

Then, using Eq. 25, where Y is C_L or C_D of the Tab. 4, and X is given by Eq. 23, we obtain the two metamodels:

$$C_L = 0{,}0425 + 0{,}0262A - 0{,}0126B + 0{,}0124AB + 0{,}0083AB^2 \quad (26)$$

$$C_D = 0{,}0883 - 0{,}0008A + 0{,}0007B + 0{,}0009AB - 0{,}0003AB^2 \quad (27)$$

By using the ANOVA technique, we used the *F*-test (Galdámez, 2002), by validating the metamodels (Eqs. 26 and 27). Table 6 present the results of ratio MQ_R/MQ_r and the *F*-test, with 95% of reliability (Tab. 5).

Table 5 – ANOVA parameters of the metamodels of the Eqs. 26 and 27.

Function	MQ_R/MQ_r	$F_{4,4}$
C_L	28,87	6,38
C_D	0,45	6,38

The metamodel of the drag coefficient (Eq. 27) has not been validated by ANOVA technique, that is the metamodel does not represent the drag coefficient changes brought about the variations of the points A and B (Eqs. 20 and 21). Physically, the drag the coefficient is not changed or it is slightly changed by camber variable. Normally, the thickness of all airfoils is more responsible by changes in C_D.

The C_L metamodel (Eq. 26) is validated by ANOVA technique, and the Eq. 26 is used in shape optimization process, *i.e.*, it is possible generate the Response Surface and using a optimize software to search the optimal point in Response Surface Curve of the Fig. 6(a), that is in the maximum C_L.

Lastly, we perform the last one simulation using the parameters obtained by optimized process. These parameters generate the red airfoil present in Fig. 3(b). The shape of the airfoil optimized is compared with shape of NACA2408 (dot line blue in Fig. 3b), that is the baseline airfoil. The lift coefficient of NACA 2408 is $C_L=0.0069$ and the Aerodynamic Efficiency $C_L/C_D=0.80$ at $Re_C=2000$. The optimized airfoil we obtain $C_L=0.0783$, *i.e.* 12.2% higher. And the $C_L/C_D = 0.886$, that is 9.56% higher.

4. CONCLUSIONS

It is noteworthy that from the metamodel obtained in Eq. 26 and validated by ANOVA technique, which is a quadratic polynomial equation, we can obtain the lift coefficient of a range of airfoils without to solve the nonlinear partial differential equations (Navier- Stokes) and continuity equation. It is given that one full simulation of the 300 physical seconds takes, approximately, 120 hours (5 days) of time processing, significant time is saved on future

projects. In the present work we shown the advantage of the IMERSPEC methodology to understand the behavior of flow over aerodynamic bodies and associating it with the RSM methodology allowed to estimate, with 95% of reliability, the optimal design of new airfoil profile, make only 10 complete CFD simulations using a high order methodology.

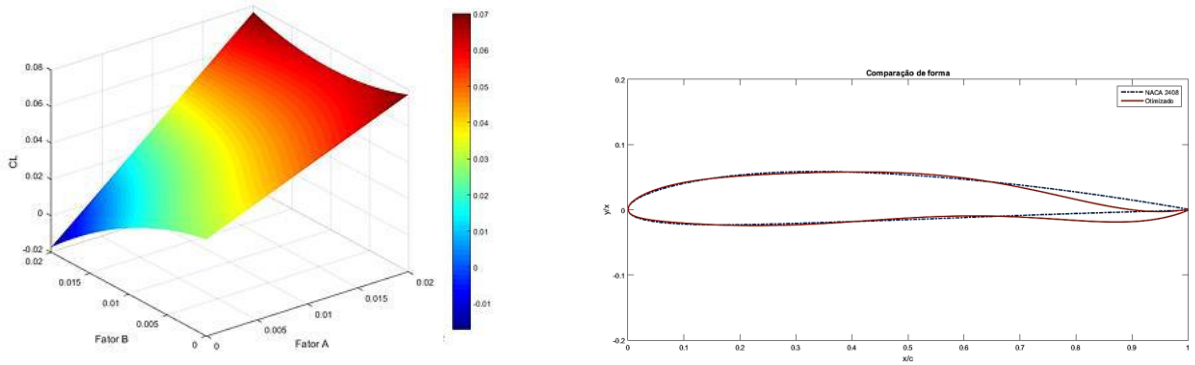

(a) (b)

Figure 6. (a) Surface response of lift coefficient and (b) Comparison between the airfoil optimized and NACA2408.

5. ACKNOWLEDGEMENTS

The authors thank the FAPEG and CNPq by financial support.

6. REFERENCES

Briggs W.L. and Henson, V.E., 1995, "*The DFT*", SIAM.

Canuto, C., Hussaini, M.Y., Quarteroni, A. and Zang, T.A., 2006, "*Spectral methods: fundamentals in single domains*", Ed: Springer-Verlag, New York, United States, 563p.

Enriquez-Remigio, S. and Silveira-Neto, A., 2007, "*A new modeling of fluid-structure interaction problems through immersed boundary method/virtual physical model (IBM/VPM)*", Proceedings of the 19th Brazilian Congress of Mechanical Engineering, Vol.1, pp. 1-10.

Griffith, B.E. and Peskin, C.S., 2005, "On the order of accuracy of the immersed boundary method: higher order convergence rates for sufficiently smooth problems", *Journal Computational Physics*, Vol.208, pp. 75-105.

Mariano, F.P., Moreira, L.Q., Silveira-Neto, A., da Silva, C.B. and Pereira, J.C.F., 2010, "A new incompressible Navier-Stokes solver combining Fourier pseudo-spectral and immersed boundary methods", *Computer Modeling in Engineering Science*, Vol.1589, pp. 1-35.

Peskin, C.S., 2002, "The immersed boundary method", *Acta Numerica*, Vol.11, pp. 479–517.

Uhlmann, M., 2005, "An immersed boundary method with direct forcing for the simulation of particulate flows", *Journal of Computational Physics*, Vol.209, pp. 448-476.

Barros Neto, B., Scarminio, I., & Bruns, R. (2001). "*Como fazer experimentos: pesquisa e desenvolvimento na ciência e na indústria*". Campinas : Editora da Unicamp.

Galdámez, E. V. (2002). "*Aplicação das técnicas de planejamento e análise de experimentos na melhoria da qualidade de um processo de fabricação de produtos plásticos*". São Carlos: Dissertação de mestrado - Escola de engenharia de São Carlos da Universidade de São Paulo.

Monteiro, M. L. (2018). "*Aplicação da metodologia da superfície de resposta para otimização de perfis aerodinâmicos utilizando a metodologia IMERSPEC*". Goiânia: Projeto final de curso – Escola de Engenharia Mecânica, Elétrica e Computação da Universidade Federal de Goiás.

7. RESPONSIBILITY NOTICE

The authors are the only responsible for the printed material included in this paper.